NUCLEAR SCIENCE AND TECHNIQUES **26**, 040404 (2015)

Parallel and optimized genetic Elman network for ^{252}Cf source-driven verification system*

FENG Peng (冯鹏),† WEI Biao (魏彪), and JIN Jing (金晶)
Key Laboratory of Opto-electronics Technology & System, Ministry of Education, Chongqing University, Chongqing 400044, China

(Received July 30, 2014; accepted in revised form October 13, 2014; published online August 20, 2015)

The ^{252}Cf source-driven verification system (SDVS) can recognize the enrichment of fissile material with the enrichment-sensitive autocorrelation functions of a detector signal in ^{252}Cf source-driven noise-analysis (SDNA) measurements. We propose a parallel and optimized genetic Elman network (POGEN) to identify the enrichment of ^{235}U based on the physical properties of the measured autocorrelation functions. Theoretical analysis and experimental results indicate that, for 4 different enrichment fissile materials, due to higher information utilization, more efficient network architecture, and optimized parameters, the POGEN-based algorithm can obtain identification results with higher recognition accuracy, compared to the integrated autocorrelation function (IAF) method.

Keywords: Nuclear noise analysis, Neutron detection, Parallel and optimized genetic Elman network, Enrichment identification

DOI: 10.13538/j.1001-8042/nst.26.040404

I. INTRODUCTION

The nuclear materials/weapons identification system (NMIS/NWIS) for nuclear safeguards is designed to measure the characteristics of fissile materials and infer with their properties or purposes. One of its important functions is to detect the enrichment of fissile materials. As we all know, the enrichment of fissile materials is the mark used to identify whether it is civilian or military and is the sign to evaluate the level of nuclear industry development. In some cases, we need external excitation to inject neutrons into the fissile material to cause a chain reaction of radiating neutrons and gamma rays. Through this, we obtain the necessary information to identify the enrichment of nuclear materials [1–4]. Active noise analysis technology based on ^{252}Cf spontaneous fission neutron sources has been developed in the past few years in China [5–8]. We have designed a ^{252}Cf source-driven verification system (SDVS) with a parallel and optimized genetic Elman network (POGEN) to identify the enrichment of ^{235}U.

II. ^{252}CF SOURCE-DRIVEN VERIFICATION SYSTEM

The measurement principle of a three-channel ^{252}Cf SDVS is shown in Fig. 1. The $1^{\#}$ channel is the ^{252}Cf spontaneous fission neutron source. It produces neutrons and gamma rays to "excitation (drive)" fissile material (^{235}U), causing a "stimulated emission (chain reaction)" with induced neutrons and gamma rays. These particles can be detected by the $2^{\#}$ channel and $3^{\#}$ channel. With a high-speed data acquisition card, all detected neutron signals from the 3 channels can be transferred into digital signals in a high-performance workstation with and large-capacity disk array.

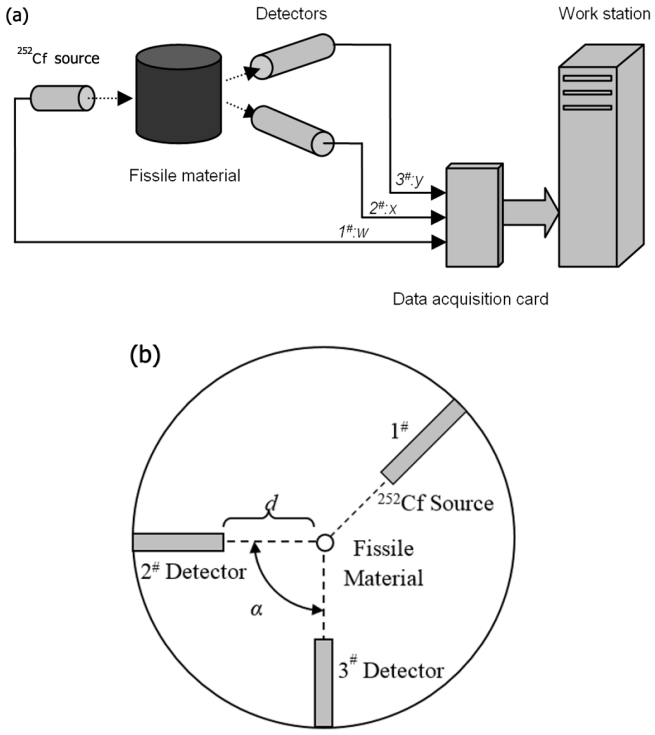

Fig. 1. Schematics of ^{252}Cf SDVS. (a) main components of SDVS; (b) position of ^{252}Cf source and two detectors.

Three channels are placed around the fissile material, as shown in Fig. 1(b). The distance d between the detector and the fissile material and the angle α between detectors can be adjusted according to the measurement requirements. According to the ^{252}Cf source-driven noise analysis (SDNA) [9–12], the SDVS calculates the autocorrelation function, cross correlation function and auto power spectral density, cross power spectrum density, and other parameters of $1^{\#}$, $2^{\#}$, $3^{\#}$-

* Supported by National Natural Science Foundation of China (Nos. 61201346, 61175005 and 61401049) and the Fundamental Research Funds for the Central Universities (No. CDJZR14125501)
† Corresponding author, coe-fp@cqu.edu.cn

channel signals: w, x and y, where w, x and y are the acquired neutron signals by the ^{252}Cf source ($1^{\#}$channel), detector 1 ($2^{\#}$ channel), and detector 2 ($3^{\#}$ channel), respectively. The SDVS uses these parameters to analyze the characteristics of fissile material. Then, the enrichment of ^{235}U can be determined.

III. AUTOCORRELATION FUNCTION OF DETECTOR CHANNEL SIGNAL

Here we use the signal x of $2^{\#}$ channel as an example. According to the SDNA method, the autocorrelation function of the detector channel signal can be expressed as Ref. [2, 3],

$$R_{xx}(\tau) = E[x(t_1)x(t_2)]|_{\tau=t_2-t_1} = C_{xx}(\tau) + \overline{x}\overline{x}, \quad (1)$$

where the autocovariance of signal x is

$$C_{xx}(\tau) = \varepsilon_x^2 \left[\overline{v_0(v_0-1)} + \frac{\overline{v_0}\overline{v(v-1)}}{\overline{v}\alpha\Lambda}\right] \frac{F_0}{2\alpha\Lambda^2} \mathrm{e}^{-\alpha|\tau|}. \quad (2)$$

and the average count rate of induced neutrons is

$$\overline{x} = \varepsilon_x \frac{\overline{v_0}F_0}{\alpha\Lambda}. \quad (3)$$

From the point reactor model of induced fission, the mean ^{252}Cf source fission rate is

$$F_0 = \frac{\alpha\Lambda\overline{v}F}{\overline{v_0}}, \quad (4)$$

where ε_x is the detection efficiency of the detector channel, $\overline{v_0}$ denotes the mean number of neutrons emitted per source fission, $\overline{v}$ is the expected number of neutrons emergent from induced fission, F is the mean system fission rate, α denotes the prompt neutron fission-chain decay constant, Λ is the prompt neutron generation time.

Thus, the autocorrelation function of a detector channel signal is related to the mean system fission rate and the expected number of neutrons emergent from induced fission, etc. Therefore, when the enrichment of ^{235}U in fissile material is higher, the value of autocorrelation function is larger [10, 11]. We can use this feature to identify the enrichment of ^{235}U.

Let X_k be the discrete expression of the signal x at the time sequence k, N denotes the length of the measured data block (in this work, N is 1024, the sampling interval is 1 ns). τ is the time delay. The unbiased autocorrelation function is given by Ref. [11–13].

$$R_{ii}(\tau) = \frac{1}{N-\tau} \sum_{k=0}^{N-1-\tau} X_k X_{k+\tau}. \quad (5)$$

where i represents signal channal number, i.e., $i = 1, 2, 3$.

One example of a calculated autocorrelation function $R_{ii}(\tau)$ is shown in Fig. 2. It has the following properties:

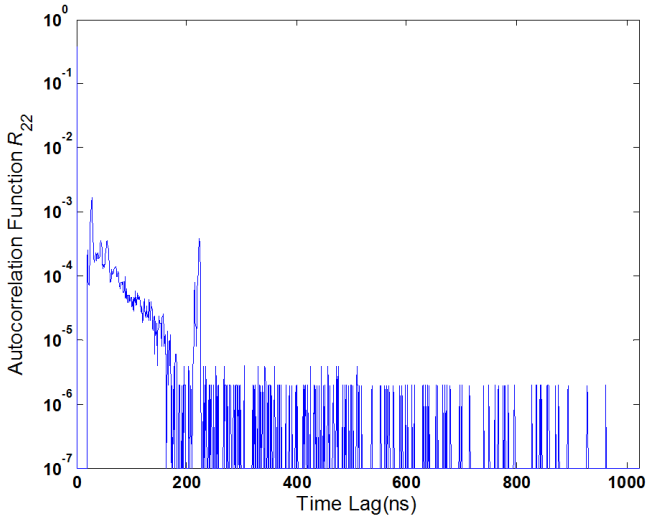

Fig. 2. (Color online) One example of autocorrelation function of $2^{\#}$ channel.

(1) $R_{ii}(\tau)$ is a delta function when the time delay is zero, i.e., $\tau = 0$. It represents the average pulse count rate in data blocks, which is normalized to 1.

(2) A time period in the region of 0 to 20 ns, in which there are no correlated counts. It reflects the dead time of signal processing electronics.

(3) A region of constant correlated counts. The autocorrelation function exhibits an exponential decrease. It is dependent on source induced and inherent fission events and background radiation. The region of 21 to 100 ns is a typical time interval, reflecting the characteristics of fissile material.

(4) It is sensitive to the enrichment of fissile material. Autocorrelation function increases with the enrichment of ^{235}U, as shown in Fig. 3. In our experiments, we use fissile materials of four different ^{235}U enrichments. The detailed parameters are listed in Table 1.

TABLE 1. Parameters of fissile materials

Net mass (kg)	U proportion	U mass (kg)	^{235}U enrichment (%)	^{235}U mass (kg)
17.520	0.99917	17.505	92.03	16.11
17.512	0.99925	17.499	87.68	15.34
17.481	0.99915	17.466	83.33	14.55
17.487	0.99920	17.473	78.98	13.80

IV. PARALLEL AND OPTIMIZED GENETIC ELMAN NETWORK

Under normal conditions, we can calculate the integral of autocorrelation functions over time to obtain their sensitivity coefficient for ^{235}U enrichment, as shown in Table 2. We can easily fit the integral value of autocorrelation and ^{235}U enrichment into a linear function $Z = f(s)$, where Z is the

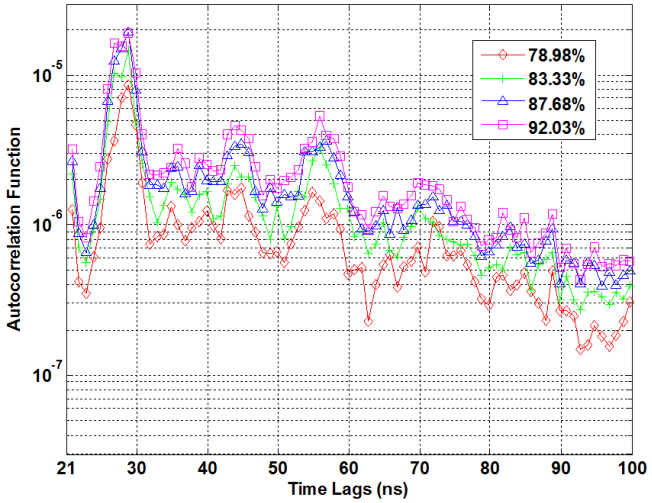

Fig. 3. (Color online) The relationship between enrichments and autocorrelation functions for ^{235}U.

^{235}U enrichment, s is the integral value of autocorrelation, and the slope of $f(s)$ is the sensitivity coefficient [14, 15]. Obviously, this kind of fit/derivation is based on ideal or semi-ideal circumstances, which means that the fissile material is not coated by Lead, Boracium, or other shielding objects, most the stimulated neutrons can travel through the highly-enriched ^{235}U and can be detected by detectors. As a pilot study, we think this assumption will not significantly influence our final results. We can use this linear function $f(s)$ to estimate the enrichment of ^{235}U in the fissile material, which we call the IAF (integral of autocorrelation functions) method for short.

TABLE 2. Integral of autocorrelation functions and sensitivity coefficient

^{235}U enrichment (%)	78.98	83.33	87.68	92.03	Sensitivity coefficient
Integral of $R_{ii}(\times 10^{-2})$	7.98	8.81	9.19	9.26	0.097

However, the accuracy of enrichment identification for the IAF method will be influenced severely by the following 2 factors:

(1) The time-varying autocorrelation function is a function of time delay. If we only refer to its integral value, we will lose information contained in the waveform. In addition, different time intervals have different sensitivities on enrichment. In the SDVS, the sensitivity is mainly reflected in the typical time interval. Therefore, direct integration will reduce the identification accuracy.

(2) Due to the existence of statistical fluctuation, autocorrelation function curves overlap when the enrichment gap is small, as shown in Fig. 3. This will impact the recognition accuracy with a significant drift on enrichment. As the integration cannot be a good solution to this problem, the statistical fluctuation limits the enrichment resolution of the SDVS.

Another disadvantage is that the integral value of autocorrelation cannot directly depict the enrichment of fissile materials. We need to design an appropriate identification mechanism which has the ability to give us the recognition results more directly and can be trained by the time series of autocorrelation functions to overcome the drift caused by statistical fluctuations. This kind of approach not only maintains the integrity of the original input autocorrelation value, but also take advantage of information contained in the autocorrelation waveform.

In order to further improve identification accuracy and overcome the drawbacks mentioned above, we propose a parallel and optimized genetic Elman network (POGEN) which uses autocorrelation functions as the input feature vectors of POGEN, trains input samples, and identifies the enrichment of ^{235}U. The POGEN is divided into four blocks as shown in Fig. 4. The subnets block includes a parallel Elman network whose parameters will be optimized by a genetic algorithm. That is why the optimization block and the subnets block can be combined together in Fig. 4.

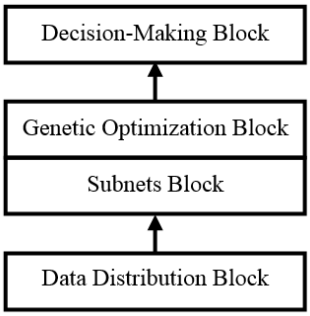

Fig. 4. Block diagram of POGEN.

The data distribution block is responsible for the allocation of the input autocorrelation functions to reduce the dimensions of the input vectors. It contains a series of multi-point random sampling (MPRS) operators. Each MPRS operator connects with an Elman network node in the subnets block. Its role is to randomly select points from the autocorrelation function, which forms the input vector of the corresponding node. In the new vector, the arrangement of those selected points is still based on their time sequence. It can be proven that the selection probability for each point is 1. Once the points are chosen, the MPRS operator gives the node a fixed address label of those points. Each node has a fixed address label during the training process and the identification process. This means the input of a node always comes from those addresses indicated by its fixed address label. An illustration of one example of MPRS is shown in Fig. 5(a), where each MPRS operator chose 5 autocorrelation values, connected them with one Elman node, and distributed all the autocorrelation values into 16 Elman nodes.

The subnets block consists of a series of parallel nodes. Each node, which can also be called a subnet, is a typical Elman neural network [16]. These nodes are used to allocate data so that they can train themselves in the training process and get the identification result in the recognition process.

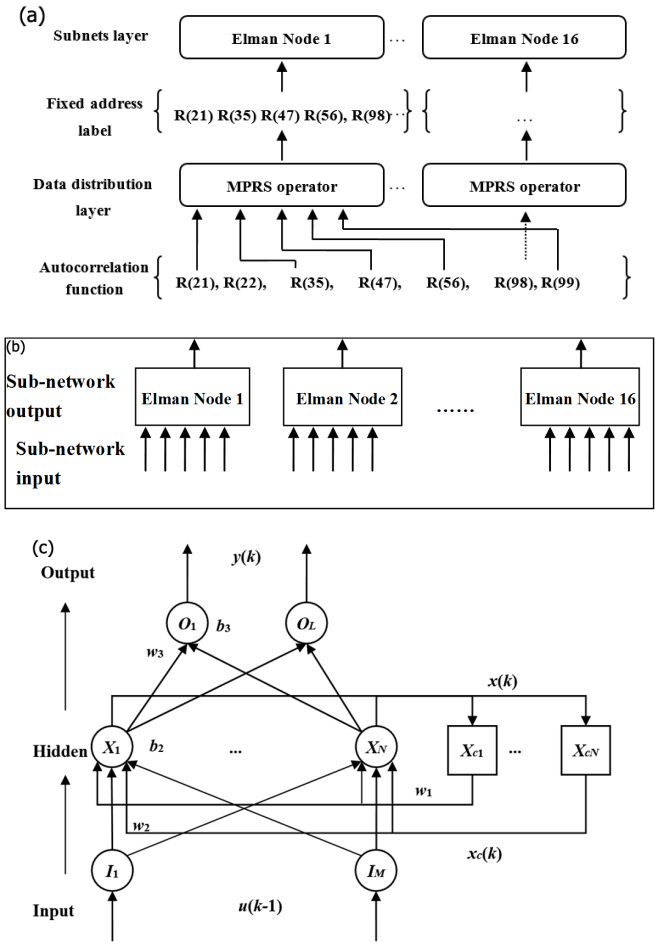

Fig. 5. Schematics of parallel and optimized genetic Elman network (POGEN). (a) The illustration of MPRS operator; (b) Illustration of Subnets block of POGEN; (c) Architecture of one Elman neural network node.

The number of nodes depends on the length of its input vector. In addition, the use of multiple nodes is helpful in reducing the uncertainty of the identification results from the dynamic recognition process.

The architecture of a typical Elman neural network is shown in Fig. 5(c). The Elman neural network uses a back-propagation algorithm (BP algorithm) for weight correction and threshold amendments [17]. As a dynamic recurrent network, it can adapt to signals with statistical fluctuations. Generally, an Elman network is divided into three layers: the input layer, hidden layer, and output layer. In addition, it has a set of "context units". There are connections between the hidden layer and these context units, which always maintain a copy of the previous values of the hidden units as a step delay operator. In Fig. 5(c), the output vector, $\boldsymbol{y}$(k), and hidden vector $\boldsymbol{x}$(k) can be represented as:

$$\boldsymbol{y}(k) = \text{purelin}[w_x \boldsymbol{x}(k)], \tag{6}$$

$$\boldsymbol{x}(k) = \text{tansig}[w_1 \boldsymbol{x}_c(k) + w_2 \boldsymbol{u}(k-1)], \tag{7}$$

where the tangent sigmoid function (tansig) and linear function (purelin) are the activation functions for the hidden layer and output layer, respectively, and are defined as:

$$\text{tansig} : \psi_t(\omega) = \frac{2}{1+\mathrm{e}^{-2t\omega}} - 1, \tag{8}$$

$$\text{purelin} : \psi_t(\omega) = t, \tag{9}$$

where the parameter t will be set to 1. The learning rule we used is the error back-propagation algorithm [18].

The feedback vector is

$$\boldsymbol{x}_c(k) = \boldsymbol{x}(k-1). \tag{10}$$

$\boldsymbol{u}(k-1)$ in Eq. (7) is the input vector. The weights of the links are w_1, w_2, and w_3. And the thresholds are b_2 and b_3.

The decision-making block is responsible for the integration of recognition results from all subnets and gives the final result. Since the all MPRS operators are the same, each Elman network node has equal weight. Therefore, this block averages the results from all nodes to get the final recognition result.

However, due to the intrinsic property of the Elman neural network, each Elman node has a certain probability of falling into a local minimum. For each Elman node, the value of the weights and thresholds in the hidden layer and output layer determines its fitness and performance in identification. Since there are many nodes in this parallel Elman network, the total probability of falling into a local minimum becomes larger, which means it's more likely that we cannot obtain the best Elman network for final identification, even if they have been trained. To solve this problem, we use a genetic algorithm to optimize the weights and thresholds in each node before the training process, what we call the genetic optimization block in Fig. 4. The flowchart of this optimization process is shown in Fig. 6. In fact, this optimization is a pre-training process on the feedforward structure of an Elman network. An individual is an array constituted by all weights and thresholds of an Elman node. Because the genetic algorithm has a strong search capability and a good macro-global optimization capability [18–20], it is more likely that the parallel Elman network can avoid falling into a local minimum and get an accurate solution after the genetic algorithm shrinks the search scope.

Through the improvements above, this network becomes a parallel and optimized genetic Elman network (POGEN). Theoretically, it has high information utilization, good generalization ability, and strong robustness. We should be able to obtain better recognition results by using the POGEN to identify the enrichment of ^{235}U.

V. EXPERIMENTAL RESULTS AND DISCUSSION

As mentioned above, we intercept the typical time interval from autocorrelation functions between 21 ns and 100 ns in the samples. Therefore, the length of each sample is 80

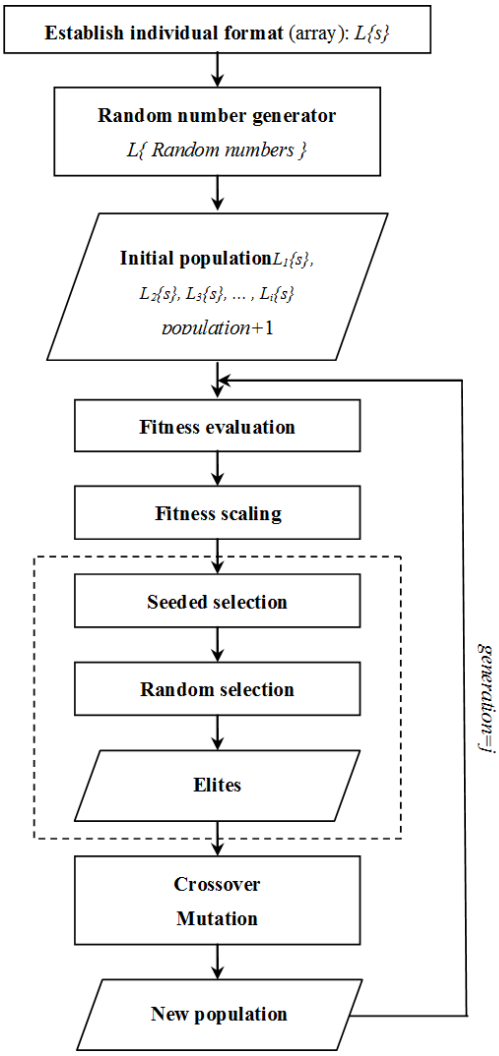

Fig. 6. Flowchart of the weights and thresholds optimization with genetic algorithm.

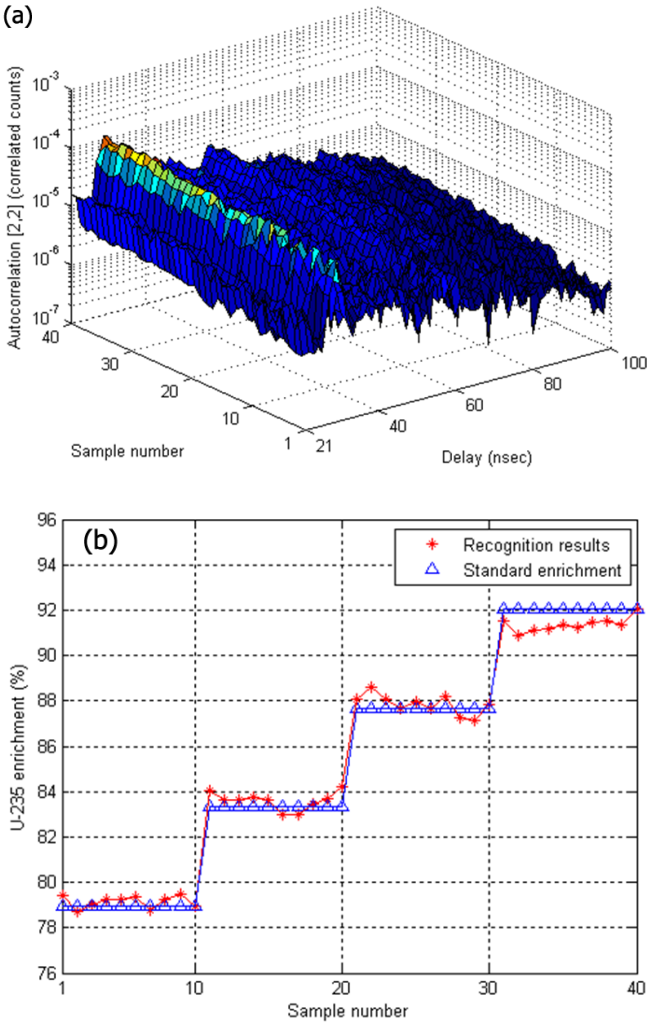

Fig. 7. (Color online) Results of identification for training sample with POGEN. (a) is the illustration for training samples, (b) is the identification results.

points. Thus, when we set the data distribution method of the MPRS operators to be 5-point random sampling, the number of Elman nodes in Fig. 5(b) is 16.

The SDVS obtains autocorrelation functions from the fissile materials of four ^{235}U enrichments (78.98%, 83.33%, 87.68%, 92.03%) as shown in Table 1. We get 10 samples for each enrichment. These 40 samples are shown in Fig. 7(a). The sample numbers are in order by their enrichments from low to high. As shown in the figure, the statistical fluctuation causes sample aliasing. We use these 40 samples to train the POGEN. We set the ^{235}U enrichments in decimal form to be training targets, such as 0.7898, 0.8333, 0.8768, and 0.9203.

Each Elman node is a three-layer network with a 'tansig' function in its hidden layer and a 'purelin' function in its output layer. The number of neurons in its hidden layer is 5, the same as in the input layer. In its output layer, there is only one neuron whose output is the ^{235}U enrichment. The POGEN uses a genetic algorithm with a population of 50 and a generation of 100 to optimize the initial threshold values and weights between layers in each node. In our experiments, the genetic fitness increases and the genetic error decreases rapidly during the genetic optimization, reducing the initial error of an Elman node to 10^{-2} before training. After 1500 iterations, the training was terminated when the convergence error reached 0.001. The total time consumption of the training and genetic optimization process is about 3 minutes with a Core Quad I7-3770 and 16G DDR3 RAM. When the training is over, all parameters of POGEN will be fixed and can be used directly to identify enrichment, i.e., no more training is needed.

For these 40 training samples, the identification results are shown in Fig. 7(b). The blue line is for standard enrichment and the red line is for recognition results. Although there are some fluctuations compared to standard enrichment, the mean square error (MSE) for the recognition results is 0.2637, which means POGEN achieves good identification results with high precision and can be used as a good candidate to identify enrichment after sufficient training.

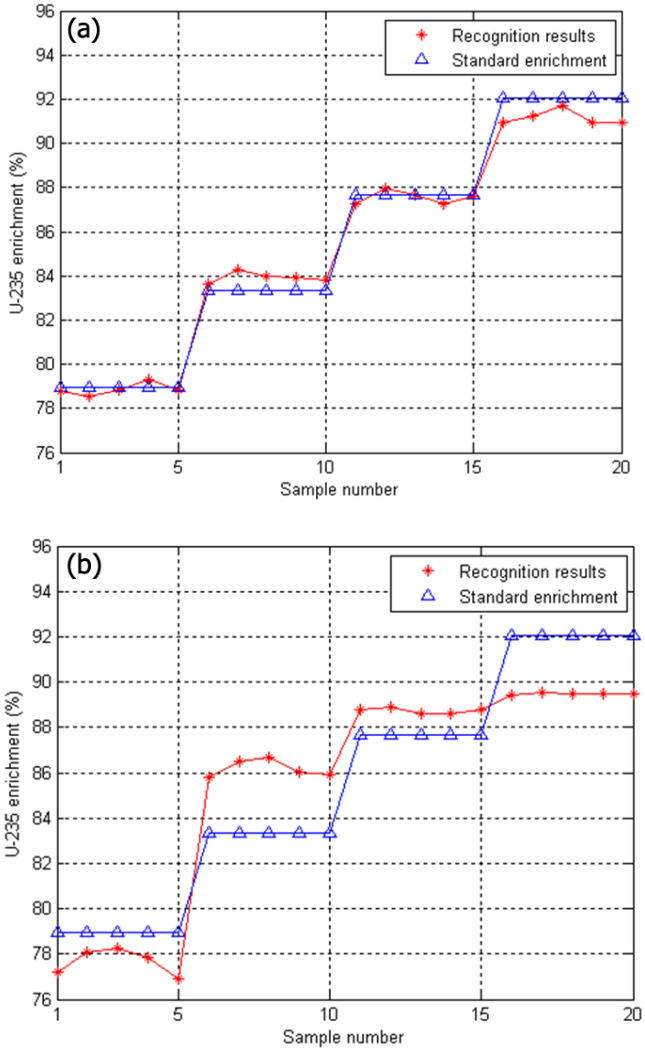

Fig. 8. (Color online) Identification results with POGEN (a) and IAF (b).

We use another 20 samples which are also selected from those 4 kinds of fissile materials (5 samples on each enrichment) to demonstrate our POGEN method. With the same parameters as mentioned above, the final identification results are shown in Fig. 8(a). Although the total identification rate is as high as 95% , the total MSE is 0.03449, which proves that the recognition accuracy is high and the identification results reach a high precision. It can be seen that the identification error is still visible, especially for the highest enrichment (sample numbers 16 to 20). Since only 40 samples are used as training samples and the left 20 samples are used for identification, the trained network can not achieve the best performance, which results in identification errors with large fluctuation. We infer that the fluctuation in the autocorrelation function of high enrichment fissile material is relatively larger than that of low enrichment fissile material, which will interfere in the training process and lead to more error in the identification results. In Fig. 7(b), this relationship is relatively clearer than it is in Fig. 8(a) because more samples are used for identification. So it is intuitive that if more data are taken into consideration, the accuracy will increase accordingly. So far, we can not get more data, especially data from different enrichments. That is why our research is just a pilot exploration.

For comparison purposes, we also list the identification results of the IAF method with the same 20 test samples. As shown in Fig. 8(b), this method cannot distinguish between the enrichment of 87.68% and 92.03% (samples number 11 to 20). Its MSE is 4.4713, which is much larger than that of the POGEN. This comparison shows that many factors will influence the identification process. The distance between different autocorrelation functions as a sole element is not enough if we want to obtain good identification results with high precision and accuracy. Although the POGEN method can get better results due to the optimization of the genetic algorithm and parallel Elman neural network, some key factors, such as shielding, position, and scattering, will obviously degrade the performance of POGEN. For future study, more relatively realistic experiments and a more comprehensive identification model need to be taken into consideration in order to further improve this method.

VI. CONCLUSION

Based on the intrinsic relationship between the autocorrelation function and the enrichment of fissile materials, we propose a parallel and optimized genetic Elman network in order to further improve the identification accuracy of autocorrelation functions with different enrichment ^{235}U. The data distribution mechanism of the POGEN improves information utilization, while maintaining generalization ability. The genetic algorithm optimizes the parallel Elman network robustness. With data acquired from the SDVS system, experimental results show that the POGEN-based identification approach achieves better recognition accuracy and higher enrichment resolution compared to the IAF-based method. Furthermore, comprehensive research on the effects of the number of Elman nodes, input vector dimensions and the time-consumption of iteration to further improve the performance of POGEN-based identification approaches is on the way.

[1] Valentine T E. Review of subcritical source-driven noise analysis measurements. The U.S. department of energy report, ORNL/TM-1999/288, 1999, 1–15. DOI: 10.2172/15041

[2] Mattingly J K T, Mihalczo J T, Mullens J A, *et al*. Physical and mathematical description of nuclear weapons identification system (NWIS) signatures. The U.S. department of energy report, Y/LB-15946-R3, 1997, 1–43. DOI: 10.2172/1878

[3] Luo Z L and Luo A R. Physics of experimental reactor. Beijing (China): Atomic Energy Press, 1987. (in Chinese)

[4] Liu C G and Wu J. An introduction of verification technology of nuclear arms control. Beijing (China): National Defense Industry Press, 2007. (in Chinese)

[5] Wei B, Yang F, Feng P, *et al*. A new NMIS characteristic signature acquisition method based on time-domain fission correlation spectrum. Nucl Power Eng, 2014, **35**: 10–13. (in Chinese)

[6] Zhou M, Wei B, Mi D L, *et al*. Simulation study for high enriched-uranium components with reflector based on ^{252}Cf source-driven noise analysis method. High Power Laser Part Beam, 2014, **26**: 050101. DOI: 10.11884/HPLPB201426.050101

[7] Feng P, Liu S Y, Wei B, *et al*. Simulation and experimental study of a random neutron analyzing system with ^{252}Cf neutron source. Nucl Sci Tech, 2011, **22**: 39–46.

[8] Zhou M, Wei B, Yang F, *et al*. Simulation study of neutrons time-correlated coincidence count for uranium components based on ^{252}Cf source-driven noise analysis method. Nucl Tech, 2013, **36**: 060202. (in Chinese) DOI: 10.11889/j.0253-3219.2013.hjs.36.060202

[9] Mattingly J K, Valentine T E and Mihalczo J T. NWIS measurements for uranium metal annular casting. The U.S. department of energy report, No. Y/LB-15,971, Oak Ridge Y-12 Plant, 1998, 1–25.

[10] Mattingly J K, Valentine T E, Mihalczo J T, *et al*. Enrichment and uranium mass from NMIS for HEU metal. Proceedings of the 41st Instrument for Nuclear Materials Management Annual Meeting, 2000, 51–55.

[11] Mihalczo J T, Mullens J A, Mattingly J K, *et al*. Physical description of nuclear materials identification system (NMIS) signatures. Nucl Instrum Meth A, 2000, **450**: 531–555. DOI: 10.1016/S0168-9002(00)00304-1

[12] Jin J. Signal processing and recognition of ^{252}Cf neutron source spectrum analysis system for nuclear arms control verification based on photoelectric detection. Ph.D. Thesis, Chongqing University, 2011. (in Chinese)

[13] Pozzi S A and Segovia J. ^{252}Cf source-correlated transmission measurements and genetic programming for nuclear safeguards, Nucl Instrum Meth A, 2002, **491**: 326–341. DOI: 10.1016/S0168-9002(02)01120-8

[14] Liu L X, Xia X B, Sheng Y X, *et al*. Effects of scattered neutrons on the neutron radiation field generated by Cf-252 neutron source with a shield. Nucl Tech, 2013, **36**: 100201. (in Chinese) DOI: 10.11889/j.0253-3219.2013.hjs.36.100201

[15] Xu D P, Yao Z E, Feng H Y, *et al*. Preliminary study on biological effects of pea seeds (*Pisum sativum* L.) induced by ^{252}Cf neutron source. Nucl Tech, 2013, **36**: 110207. (in Chinese) DOI: 10.11889/j.0253-3219.2013.hjs.36.110207

[16] Portegys T E. A maze learning comparison of Elman, long short-term memory, and Mona neural networks. Neural Networks, 2010, **23**: 306–313. DOI: 10.1016/j.neunet.2009.11.002

[17] Ciarlini P and Maniscalco U. Wavelets and Elman neural networks for monitoring environmental variables. J Comput Appl Math, 2008, **221**: 302–309. DOI: 10.1016/j.cam.2007.10.040

[18] Schmidhuber J. Deep learning in neural networks: an overview. Neural Networks, 2015, **61**: 85–117. DOI: 10.1016/j.neunet.2014.09.003

[19] Pham D T and Karaboga D. Training Elman and Jordan networks for system identification using genetic algorithms. Artif Intell Eng, 1999, **13**: 107–117. DOI: 10.1016/S0954-1810(98)00013-2

[20] Araujo L, Zaragoza H, Pérez-Agüera J R, *et al*. Structure of morphologically expanded queries: A genetic algorithm approach. Data Knowl Eng, 2010, **69**: 279–289. DOI: 10.1016/j.datak.2009.10.010